

Supporting Information

Selective oxidation of polyolefins to carbon monoxide by photo-assisted catalysts

Hiroki Nagai^a, Hiroaki Kaneko^a, Yohei Cho^a, Akira Yamaguchi^a, Masahiro Miyauchi^{a*}

^a Department of Materials Science and Engineering, School of Materials and Chemical Technology, Institute of Science Tokyo, 2-12-1 Ookayama, Meguro-ku, Tokyo 152-8552, Japan.

Contents of Supporting Information

Figure S1. Experimental setup for the degradation of *n*-octane (C₈H₁₈).

Figure S2. Experimental setup for the degradation of LDPE.

Figure S3. TEM image of fabricated Rh/MCM-41 (a-c) using an ion slicer, and those of Rh/SrTiO₃ (d, e).

Figure S4. EDS spectra of Rh/MCM-41 (a) and Rh/SrTiO₃ (b).

Figure S5. TEM images of Rh/MCM-41 fabricated using commercial MCM-41 using an ion slicer (a), and its high-resolution image (b).

Figure S6. BET isotherm of Rh/MCM-41 (a), and mesopore distribution of Rh/MCM-41 (b).

Figure S7. The amount of gas products through C₈H₁₈ degradation for various conditions.

Figure S8. The amount of gas produced from C₈H₁₈ degradation using Rh/MCM-41 with different Rh loadings.

Figure S9. The amount of gas products through C₈H₁₈ degradation for various mesoporous SiO₂.

Figure S10. The mass spectra of liquid products from C₈H₁₈.

Figure S11. The amount of gas produced from C₈H₁₈ degradation using Rh/MCM-41 (a) and Rh/SrTiO₃ (b) under different light intensities.

Figure S12. The action spectrum of Rh/SrTiO₃.

Table S1. (a) Temperatures of C₈H₁₈ solution dispersed with catalysts under UV irradiation, and (b) surface temperatures of catalysts under UV irradiation in dried atmosphere.

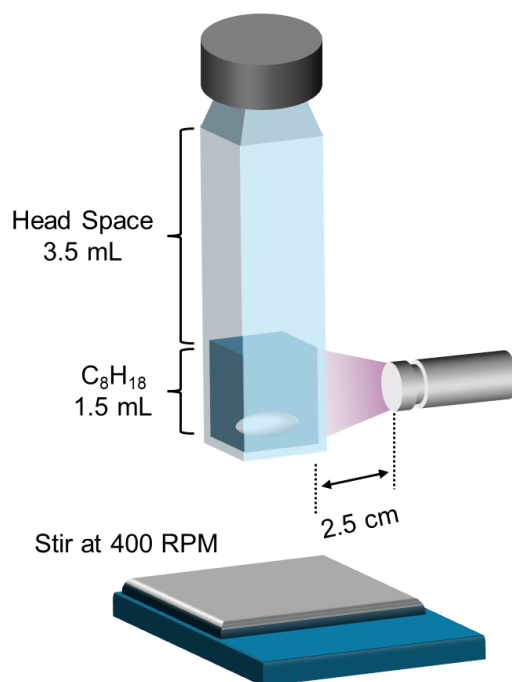


Figure S1. Experimental setup for the degradation of *n*-octane (C_8H_{18}). Catalyst powder was dispersed in the liquid of C_8H_{18} .

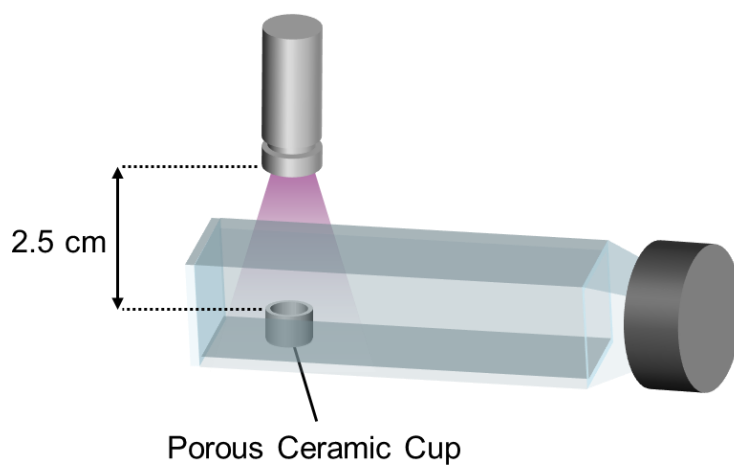


Figure S2. Experimental setup for the degradation of LDPE. The mixture of catalyst powder and LDPE was placed on the ceramics cup.

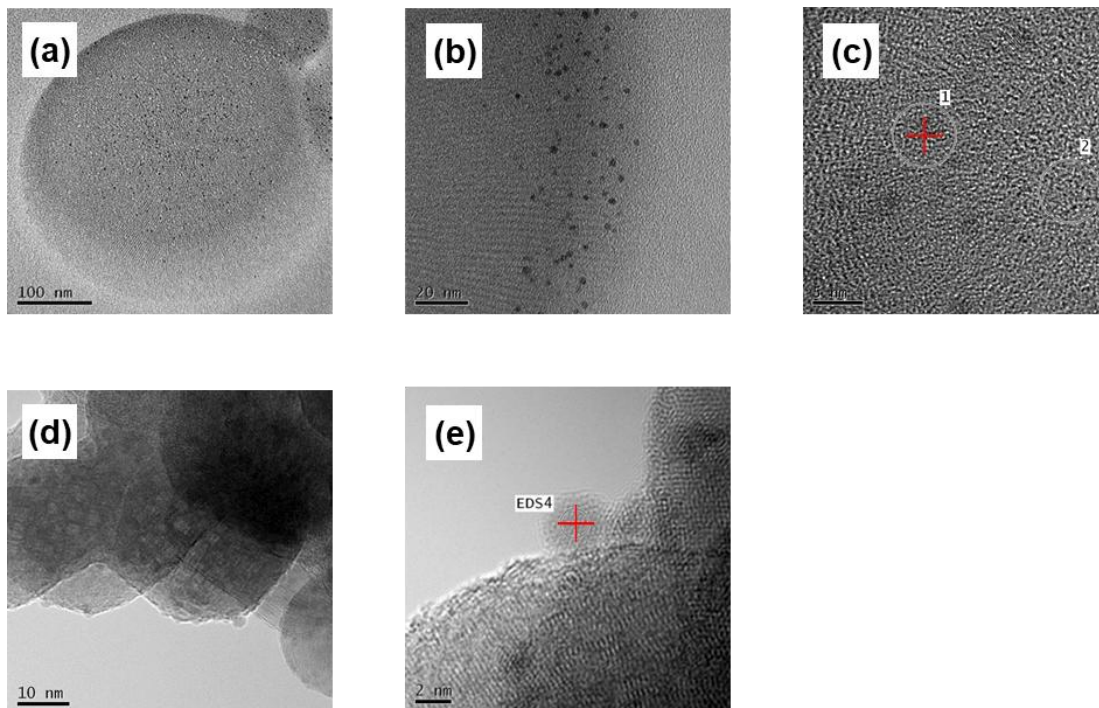


Figure S3. TEM images of Rh/MCM-41 (a- c), and those of Rh/SrTiO₃ (d, e). Red crosses in panel (c) and (e) represent the point of EDS analysis of Figure S4.

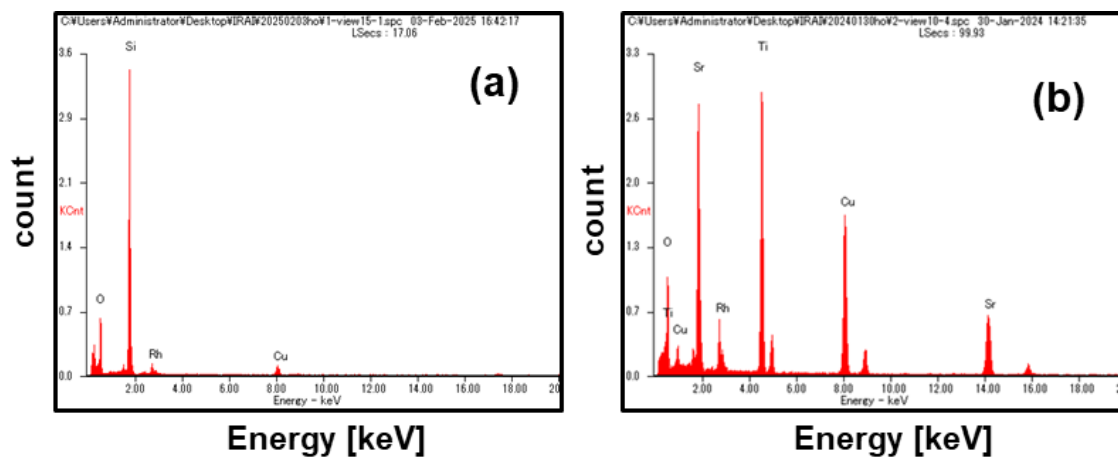


Figure S4. EDS spectra of Rh/MCM-41 (a), and Rh/SrTiO₃ (b). Electron beam was focused on the red crosses in Figure S3. In both figures, Rh signals were seen.

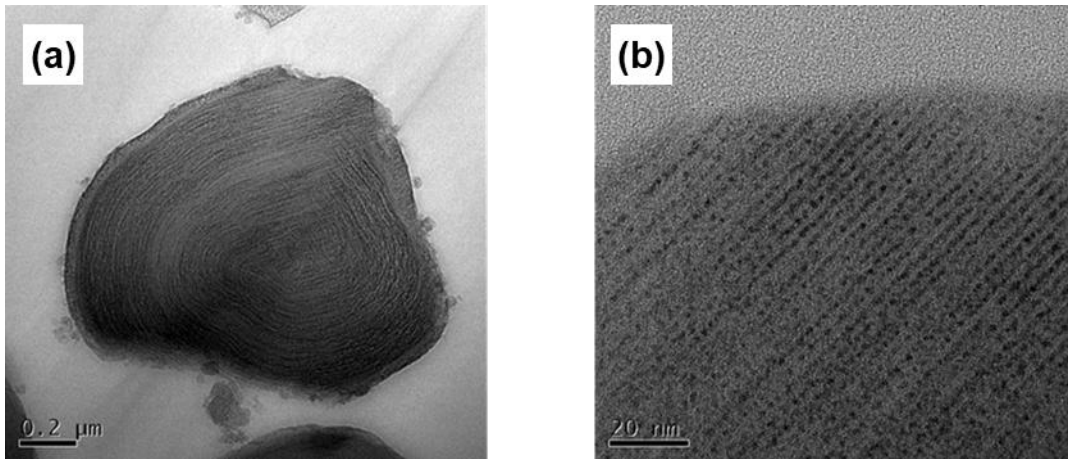


Figure S5. TEM images of Rh/MCM-41 fabricated using commercial MCM-41 using an ion slicer (a), and its high-resolution image (b).

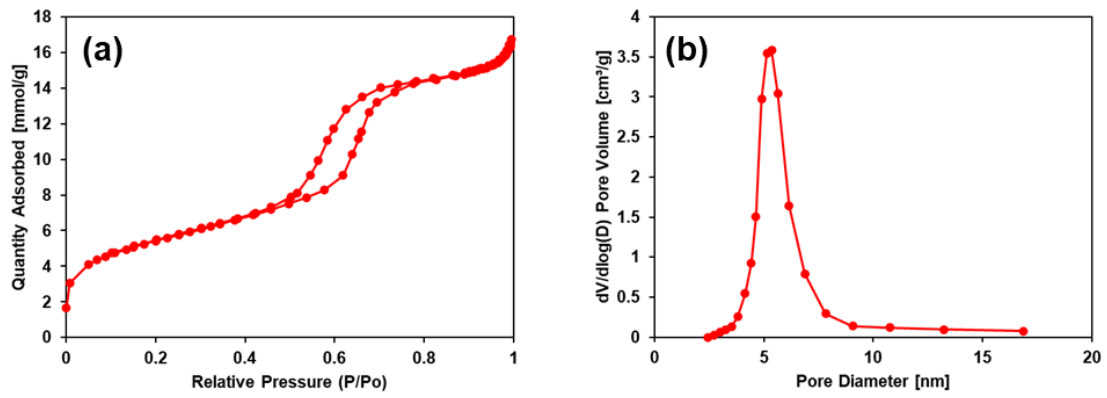


Figure S6 BET isotherm of Rh/MCM-41 (a), and mesopore distribution of Rh/MCM-41 (b).

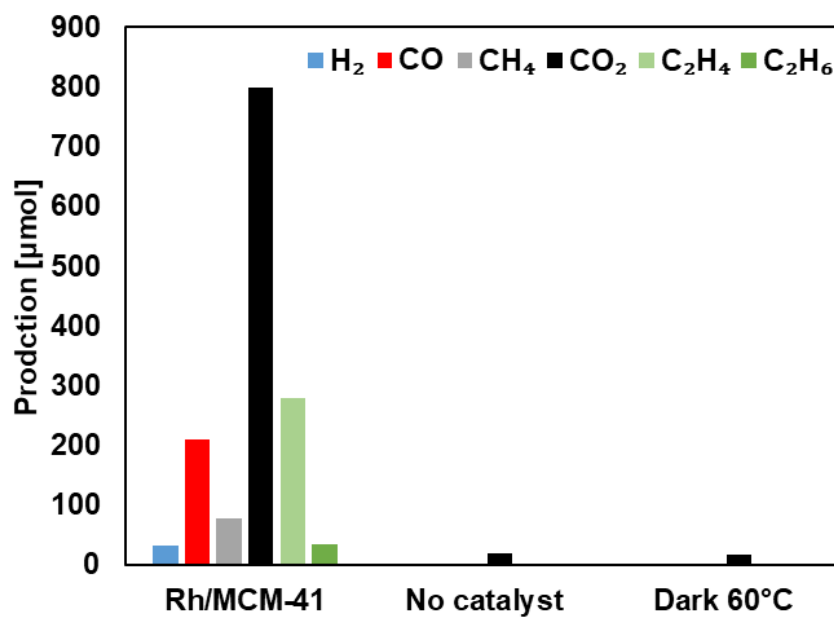


Figure S7. The amount of gas products through C₈H₁₈ degradation for various conditions.

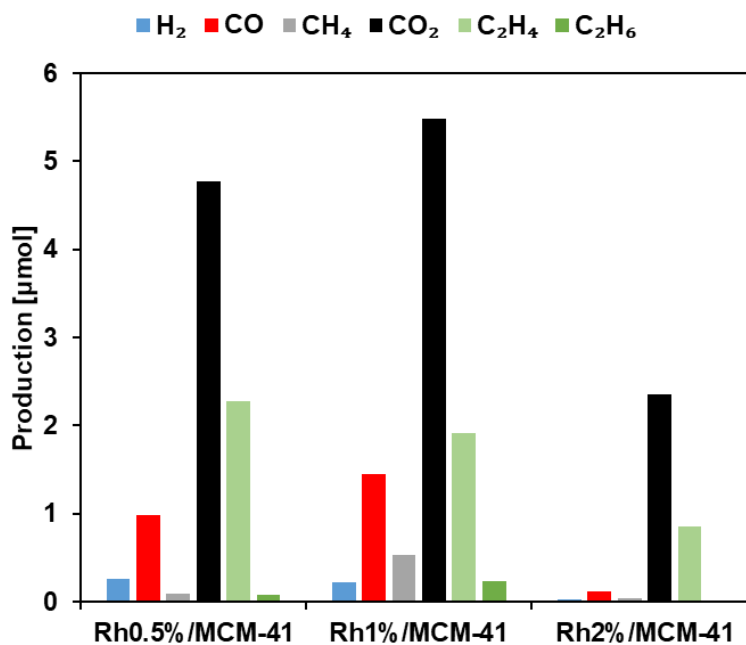


Figure S8. The amount of gas produced from C₈H₁₈ degradation using Rh/MCM-41 with different Rh loadings.

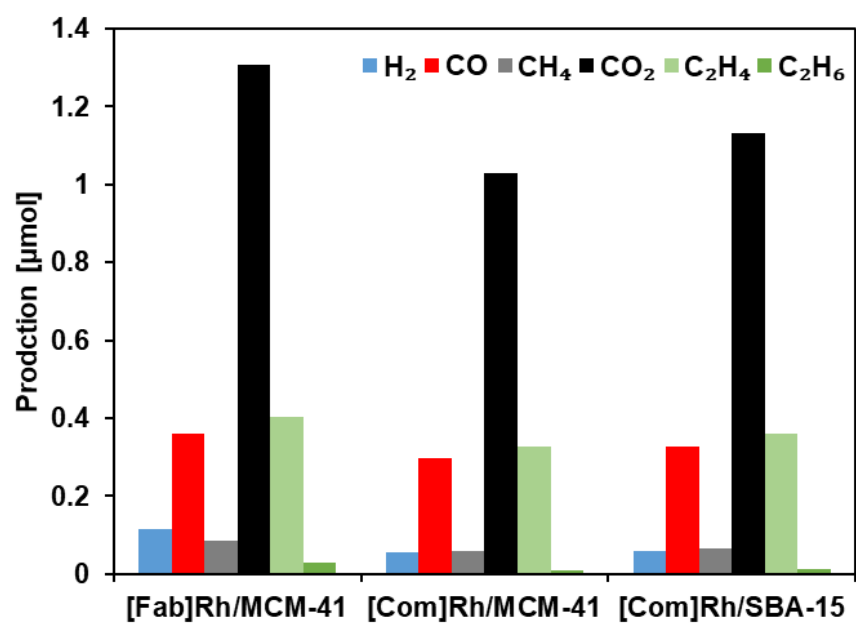


Figure S9. The amount of gas products through C₈H₁₈ degradation for various Rh-loaded mesoporous SiO₂.

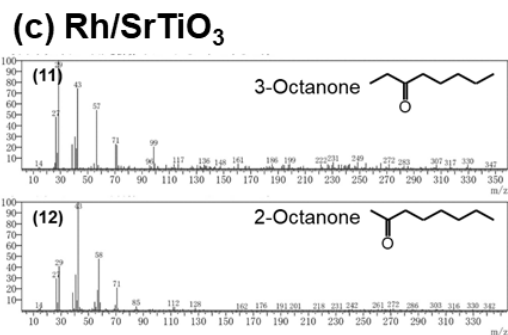
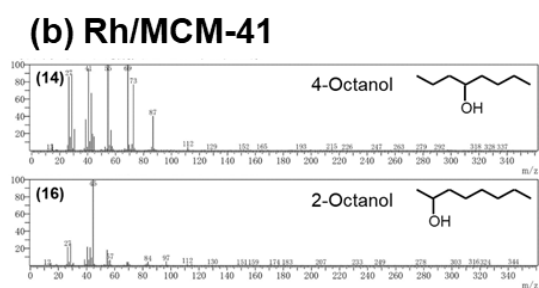
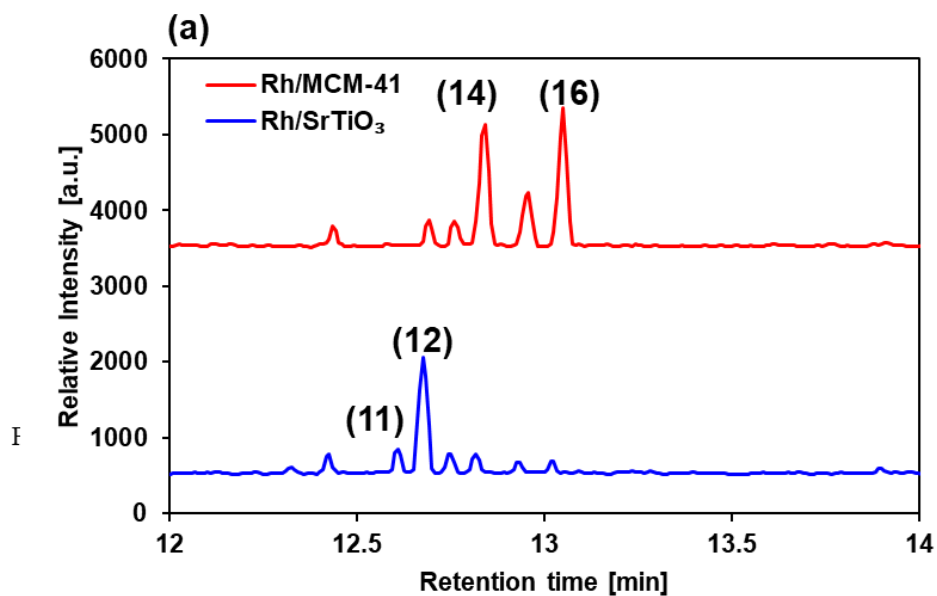


Figure S10. The mass spectra of liquid products from C₈H₁₈.

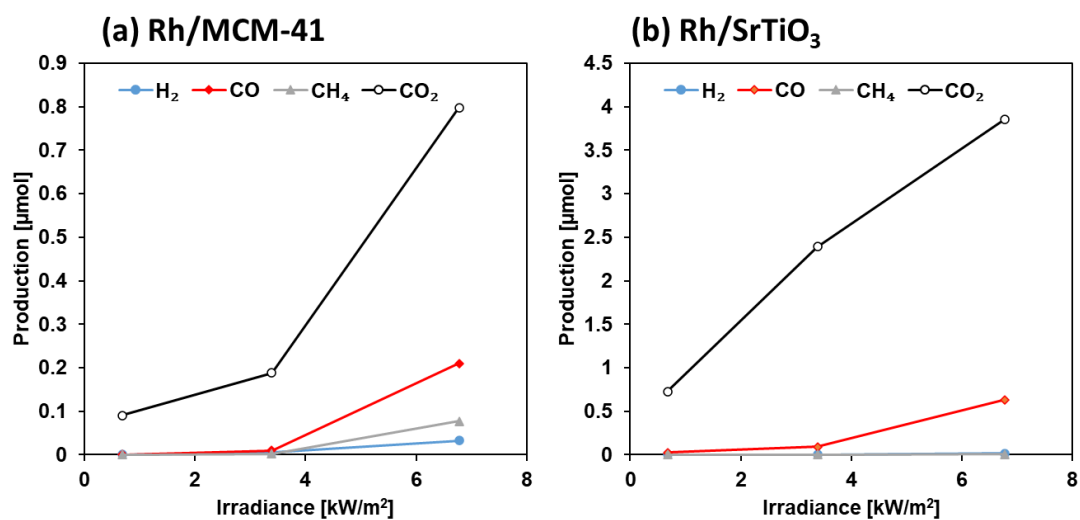


Figure S11. The amount of gas produced from C_8H_{18} degradation using Rh/MCM-41 (a) and Rh/SrTiO₃ (b) under different light intensities. Oxygen gas condition: $O_2/(O_2+N_2) = 5\%$.

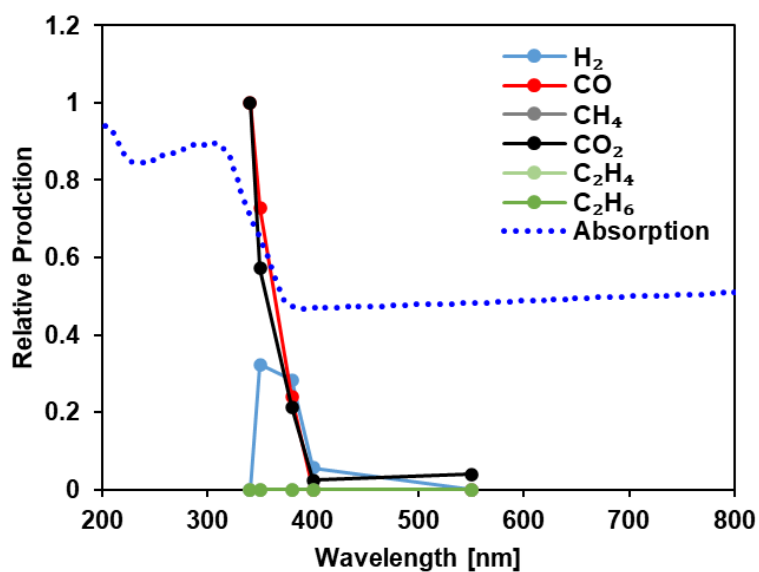


Figure S12. The action spectrum of Rh/SrTiO₃, where oxygen gas condition was 100%.

Table S1. (a) Temperatures of C₈H₁₈ solution dispersed with catalysts under UV irradiation, and (b) surface temperatures of catalysts under UV irradiation in dried atmosphere.

(a) The temperatures of C₈H₁₈ under UV irradiation measured by a thermocouple.

	Rh/MCM-41	Rh/SrTiO ₃
Temperature [°C]	60.1	59.5

(b) The surface temperatures under UV irradiation measured by a radiative thermometer.

	Rh/MCM-41	Rh/SrTiO ₃
1 st time [°C]	137.5	157.5
2 nd time [°C]	141	157
3 rd time [°C]	141.5	152.5
Average [°C]	140	156